

PAPER

# Emergence of field-induced memory effect in spin ices



To cite this article: Pramod K Yadav *et al* 2023 *J. Phys.: Condens. Matter* **35** 495601

View the [article online](#) for updates and enhancements.

## You may also like

- [Simulation of the AC susceptibility for nano-ferromagnetic materials](#)  
Wang Wang and An Du
- [Magnetic ordering of the martensite phase in Ni–Co–Mn–Sn-based ferromagnetic shape memory alloys](#)  
Sudip Kumar Sarkar, Sarita Ahlawat, S D Kaushik et al.
- [Pressure effect on magnetic phase transition and spin-glass-like behavior of GdCo<sub>2</sub>B<sub>2</sub>](#)  
Guang-Hui Hu, , Ling-Wei Li et al.

# Emergence of field-induced memory effect in spin ices

Pramod K Yadav<sup>1,\*</sup> , Rajnikant Upadhyay<sup>2</sup> , Rahul Kumar<sup>3</sup>, Pavan Nukala<sup>1</sup> and Chandan Upadhyay<sup>2</sup> 

<sup>1</sup> Centre for Nano Science and Engineering, Indian Institute of Science, Bangalore 560012, India

<sup>2</sup> School of Materials Science and Technology, Indian Institute of Technology (Banaras Hindu University), Varanasi 221005, India

<sup>3</sup> School of Advanced Materials and Chemistry and Physics of Materials Unit, Jawaharlal Nehru Centre for Advanced Scientific Research, Bangalore 560064, India

E-mail: [pramodyadav@iisc.ac.in](mailto:pramodyadav@iisc.ac.in) and [pyadav.rs.mst13@itbhu.ac.in](mailto:pyadav.rs.mst13@itbhu.ac.in)

Received 2 February 2023, revised 31 July 2023

Accepted for publication 16 August 2023

Published 7 September 2023



## Abstract

Out-of-equilibrium investigation of strongly correlated materials deciphers the hidden equilibrium properties. Herein, we have investigated the out-of-equilibrium magnetic properties of polycrystalline Dy<sub>2</sub>Ti<sub>2</sub>O<sub>7</sub> and Ho<sub>2</sub>Ti<sub>2</sub>O<sub>7</sub> spin ices. Our experimental findings reveal the emergence of magnetic field-induced anomalous hysteresis observed solely in temperature- and magnetic field-dependent AC susceptibility measurements. The observed memory effect (anomalous thermomagnetic hysteresis) exhibits a strong dependence on both thermal and non-thermal driving variables. Owing to the non-collinear spin structure, the applied DC bias magnetic field produces quenched disorder sites in the cooperative Ising spin matrix and suppresses the spin–phonon coupling. These quench disorders create a dynamic spin correlation, having slow spin relaxation and quick decay time, which additionally contribute to AC susceptibility. The initial conditions and measurement protocol decide the magnitude and sign of this dynamical term contributing to AC susceptibility. It is being suggested that such out-of-equilibrium properties arise from the combined influences of geometric frustration, disorder, and the cooperative nature of spin dynamics exhibited by these materials.

Supplementary material for this article is available [online](#)

Keywords: spin ice, memory effect, pyrochlore oxides, magnetic frustration

(Some figures may appear in colour only in the online journal)

## 1. Introduction

Armed with an in-depth understanding of the exciting properties of topological materials, new design concepts are being developed to emulate alternate computing devices [1–4]. Geometrically frustrated Dy<sub>2</sub>Ti<sub>2</sub>O<sub>7</sub> (DTO) and Ho<sub>2</sub>Ti<sub>2</sub>O<sub>7</sub> (HTO) pyrochlore oxides are one of them and are known for their low-temperature exotic behavior. In these materials, Ho/Dy ions occupy the lattice of corner-sharing tetrahedra

of the Fd  $\bar{3}m$  space group. A strong crystal field constrains the Ho/Dy spin along their local  $\langle 111 \rangle$  crystallographic direction, such that each spin points towards the centre of the corner shared tetrahedron and behaves Ising-like [5, 6]. Below 4 K, long-range dipolar interactions stabilize the spin ice state where spins follow a 2in-2out correlation in each tetrahedron [7, 8]. Based on previous findings, spin dynamics of these materials can be categorized into three regimes: (i) a high-temperature paramagnetic phase at temperatures  $>13$  K where dynamics is well-described by an Arrhenius law; (ii) an intermediate regime from 2 to 13 K where the dominant relaxation mechanism is single-ion quantum tunnelling leading to

\* Author to whom any correspondence should be addressed.

a temperature-independent relaxation rate; and (iii) a spin-ice regime below 2 K, where relaxation is driven by the creation and diffusion of magnetic monopoles and the relaxation time increases as the temperature is reduced until the dynamics freeze out for experimental timescales around 0.6 K [7, 9–12].

Recently, Samarakoon *et al* performed a low-temperature ultrasensitive magnetic noise experiment on DTO, revealing that out-of-equilibrium spin dynamics show cooperative and memory effect behavior [13]. The observed effect is associated with the formation of the magnetic monopoles in the spin ice ground state, suppressing the dynamics of the quarter of spins [14, 15]. Savary and Balents [16] investigated the role of disorder in spin ices and proposed the formation of disorder-induced spin liquid-like states in HTO. In a previous study, we also observed anomalous thermal hysteresis in DC magnetic field biased AC susceptibility measurements, which shows a strong dependence on driving frequency [17]. However, the origin and responsible phenomena of observed hysteresis, existed up to the high-temperature paramagnetic phase, is still unknown. Herein, we have systematically investigated the magnetic and dielectric properties of DTO and HTO in different measurement protocols. Experimental findings reveal that dynamic magnetic properties in these materials have distinct behavior in equilibrium and non-equilibrium states, which have been discussed in detail with their possible origins.

## 2. Experimental details

High-quality polycrystalline  $\text{Dy}_2\text{Ti}_2\text{O}_7$  (DTO) and  $\text{Ho}_2\text{Ti}_2\text{O}_7$  (HTO) samples have been used for the magnetic and dielectric measurements. Samples synthesis, phase purity, and their structural details have already been reported in [18–20]. Magnetic measurements are performed using Magnetic Properties Measurement System (MPMS-3)<sup>®</sup> (Quantum Design, Inc.) USA. The samples used were powder and mounted in a brass holder for the measurements. The temperature sweep rate was kept fixed at  $1.5 \text{ K min}^{-1}$  while varying the other non-thermal variables for all the temperature-dependent measurements. Low-temperature magnetodielectric measurements of DTO were performed using an Agilent E4980A LCR meter interfaced with Physical Properties Measurement System (PPMS-3)<sup>®</sup> (Evercool Quantum Design, Inc.) USA.

## 3. Results

Figures 1(a) and (b) shows the temperature-dependent real part of AC susceptibility ( $\chi'(T)$ ) measured for DTO in field-cooled cooling (FCC) and field-cooled warming (FCW) mode for varying AC variables. Figure 1(a) illustrates the  $\chi'(T)$  behavior in FCC and FCW mode measured at 1.5 Oe AC amplitude ( $H_{ac}$ ) for different frequencies ( $f$ ). Below 4 K, FCC and FCW of  $\chi'(T)$  show a weak frequency-dependent thermal hysteresis defined as  $\Delta\chi'(T) = \chi'(T)_{\text{FCC}} - \chi'(T)_{\text{FCW}}$ . Herewith, below 2.4 K, a frequency-dependent crossover in  $\Delta\chi'(T)$  is observed for the measured frequency range. For clarity, we denote this

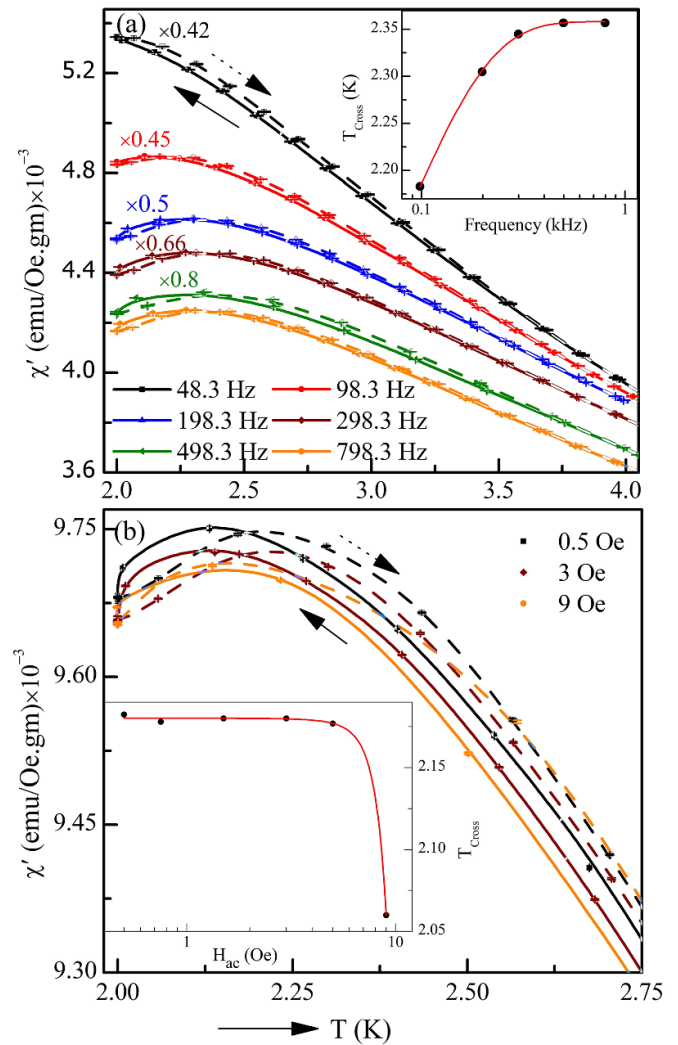


**Figure 1.** For  $\text{Dy}_2\text{Ti}_2\text{O}_7$  (a) Temperature-dependent real part of AC susceptibility ( $\chi'$ ) measured in FCC (solid symbol (with line as a guide to the eye)) and FCW (open symbol (with dashed line as a guide to the eye)) mode at 1.5 Oe AC amplitude for different frequencies. Inset shows the variation in the crossover temperature ( $T_{\text{Cross}}$ ) with frequency. (b) Temperature-dependent  $\chi'$  measured in FCC and FCW mode at 98.3 Hz for different AC amplitudes. The inset shows the variation in the  $T_{\text{Cross}}$  with AC amplitude.

hysteresis as an anomalous hysteresis ( $\Delta\chi'_A(T)$ ). Below the crossover temperature ( $T_{\text{Cross}}$ ),  $\Delta\chi'(T)$  changes its sign, transitioning negative to positive. Additionally, with increasing frequency,  $T_{\text{Cross}}$  demonstrates a peculiar increase up to 298.3 Hz, beyond which no significant changes in  $T_{\text{Cross}}$  are observed for higher frequencies.

Figure 1(b) illustrates the FCC and FCW of  $\chi'(T)$  plot, showcasing the results obtained for selected AC amplitudes of 0.5, 3, and 9 Oe, measured at a frequency of 98.3 Hz. The corresponding  $\chi'(T)$  plot measured at different  $H_{ac}$  in FCC and FCW modes are provided in figure S1 of the supplemental information file. In this measurement, we do not observe any significant change in the magnitude of  $\Delta\chi'(T)$ , similar to the behavior observed in  $\chi'(T)$  measured at various frequencies. It has been found that the crossover temperature,  $T_{\text{Cross}}$ , exhibits

insignificant change up to 5 Oe  $H_{ac}$ , but it decreases abruptly for higher  $H_{ac}$  values. Notably, we find this crossover in  $\chi'(T)$  only, and  $T_{Cross}$  shows an inverse relationship with increasing frequency and  $H_{ac}$ . A similar thermal hysteresis behavior is noted in temperature-dependent magnetization ( $M(T)$ ) measurement, conducted in both FCC and FCW mode at different DC bias magnetic field. It has been observed that thermal hysteresis emerges below 5 K and increases as the temperature decreases without any crossover. Interestingly, a comparable  $M(T)$  behavior is also observed for HTO. The  $M(T)$  behavior of DTO and HTO are provided in figure S2 of the supplemental information file. The Inset of figures 1(a) and (b) shows the  $f$  and  $H_{ac}$  dependent variation in  $T_{Cross}$  and its fit using the exponential decay equation given by:

$$T_{Cross}(f) = A \times \exp(-R \times \chi'(f)) \quad (1)$$

$$T_{Cross}(H_{ac}) = A \times \exp(-R \times \chi'(H_{ac})). \quad (2)$$

In equations (1) and (2),  $A$  and  $R$  are the fixed variables representing the amplitude and decay constant, respectively. The derived values of  $A$  and  $R$  from  $T_{Cross}$  vs frequency fit are  $-0.58 \pm 0.024$  K and  $(1.217 \pm 0.004) \times 10^{-2}$  Oe/emu, respectively. Whereas, for  $T_{Cross}$  vs  $H_{ac}$  fit, derived values of  $A$  and  $R$  are  $(-3.68 \pm 0.05) \times 10^{-5}$  K and  $(-89.8 \pm 0.1) \times 10^{-2}$  Oe/emu, respectively. A similar measurement protocol has been followed to conduct AC  $\chi(T)$  measurement for HTO and given in figure S3 of the supplemental information file. In  $\chi'(T)$  of HTO, we do not observe any crossover within the measured  $f$  and  $H_{ac}$  range, and it exhibits similar hysteresis behavior as observed in  $M(T)$ . In the  $\chi(T)$  measurements of both DTO and HTO, the magnitudes of  $\Delta\chi'(T)$  do not show any significant change with applied  $f$  and  $H_{ac}$  AC variables. The absence of crossover in  $\chi'(T)$  of HTO is quite intriguing because both DTO and HTO structurally and magnetically mimic each other. In both compounds, Ising doublets ground state of  $Dy^{3+}$  and  $Ho^{3+}$  ions are separated from the first excited state more than 100 K due to the strong crystal field anisotropy acting along the  $\langle 111 \rangle$  direction [5, 21]. The deduced values of nearest-neighbour magnetic dipolar ( $D_{nn}$ ) and exchange ( $J_{nn}$ ) interactions are 2.35 K and  $-1.24$  K, respectively, for DTO [8] and 2.4 K and 0.5 K, respectively, for HTO [5, 12]. Due to the dominance of ferromagnetic dipolar interaction, both DTO and HTO form exotic spin ice state below 4 K. However, due to the Kramer nature of the  $Dy^{3+}$  ion, the magnitude of the local transverse field formed by magnetic ions is smaller in DTO than HTO [12, 22] It possibly leads DTO to possess a slower spin relaxation time ( $\sim$ ms) than HTO ( $\sim$ ns) [11, 23, 24]. The absence of crossover in  $\Delta\chi'(T)$  in HTO indicates that order of relaxation time of the spin dynamics also play a significant role, in addition to the effective dipolar interaction, in the observed behavior.

To get deeper insight into the observed crossover in AC  $\chi'(T)$ , we conduct AC  $\chi(T)$  measurements at various DC bias magnetic fields ( $H_{dc}$ ). Figure 2 shows the  $\chi'(T)$  measured in FCC and FCW mode for DTO at different  $H_{dc}$ . Interestingly, we noticed that  $T_{cross}$  increases with an increase in  $H_{dc}$  up to

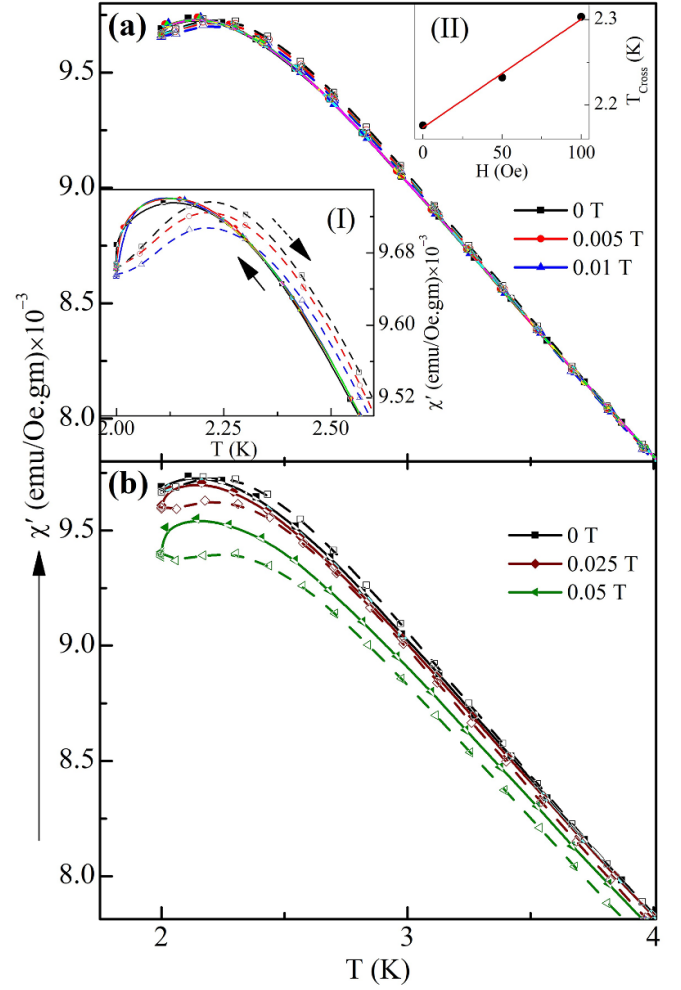


**Figure 2.** For  $Dy_2Ti_2O_7$ ; Temperature-dependent real part of AC susceptibility ( $\chi'(T)$ ) measured in FCC (solid symbol (with line as a guide to the eye)) and FCW (open symbol (with dashed line as a guide to the eye)) modes for; 0, 0.005, and 0.01 T (a) and 0, 0.025, and 0.05 T (b) DC bias magnetic field ( $H_{dc}$ ) at 98.3 Hz and 1.5 Oe AC variables. Inset (I) of figure (a) shows the zoomed view of  $\chi'(T)$  measured for 0, 0.005, and 0.01 T,  $H_{dc}$ , and Inset (II) of figure (a) shows the linear variation in crossover temperature ( $T_{Cross}$ ) with  $H_{dc}$ .

0.01 T (inset (I) of figure 2(a)). However, upon further increasing  $H_{dc}$ ,  $T_{Cross}$  expands abruptly with a simultaneous increase in the magnitude of  $\Delta\chi'_A(T)$  (figure 2(b)). Notably, for  $H_{dc}$  below 0.025 T,  $T_{cross}$  exhibits a linear relationship with  $H_{dc}$  (inset (II) of figure 2(a)).

Next, we focused on measuring  $\chi(T)$  at 0.6 T DC biased magnetic field at various  $H_{ac}$ . In previous study, we observed that  $\chi'_A(T)$  reached its maximum magnitude at 0.6 T  $H_{dc}$  and followed an exponential decaying behavior with frequency (figure S5 in the supplemental information file) [17]. Figure 3 illustrates the  $\chi'(T)$  measured in FCC and FCW modes at 0.6  $H_{dc}$  for different  $H_{ac}$ . It is worth noting that  $\chi'_A(T)$  exhibits a strong dependence on  $H_{ac}$ , and its behavior follows an exponential decay with increasing  $H_{ac}$  (inset of figure 3). A similar observation has been found for HTO (figure S4 (supplemental information file)). These findings confirm the significant influence of the AC variables on  $\chi'_A(T)$  in both

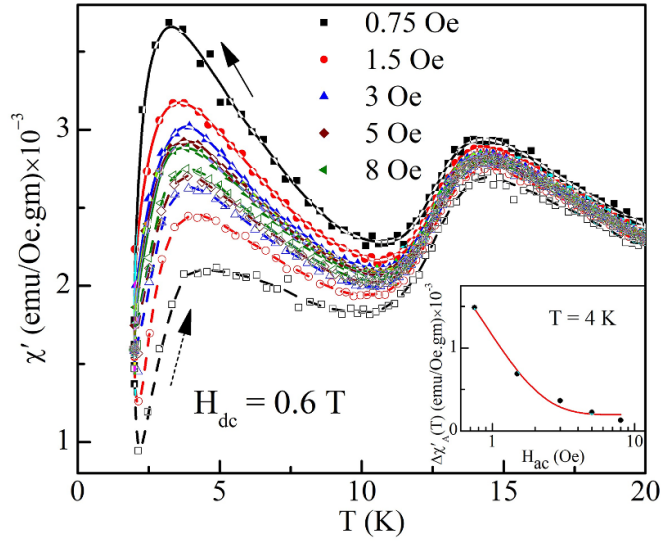


**Figure 3.** Temperature-dependent real part of AC susceptibility ( $\chi'(T)$ ) measured in FCC (solid symbol (with line as a guide to the eye)) and FCW (open symbol (with dashed line as a guide to the eye)) modes at 98.3 Hz frequency for different AC amplitudes ( $H_{ac}$ ) in the presence of 0.6 T and inset shows the exponential fit of  $H_{ac}$  dependent anomalous thermal hysteresis ( $\Delta\chi'_A(T)$ ) at 4 K.

DTO and HTO. Intriguingly, when we examined unbiased  $H_{dc}$  condition, the magnitudes of  $\Delta\chi(T)$  do not show any significant changes with AC variables in both compounds.

In order to investigate the potential origin of the anomalous change in the thermal hysteresis and its sensitivity to temperature sweep rates for both unbiased and biased  $H_{dc}$ , we performed AC  $\chi(T)$  in FCC and FCW modes at different temperature sweep rates. The figure 4 depicting the  $\chi'(T)$  in FCC and FCW modes measured at different temperature sweep rates. Notably, the magnitude of  $\Delta\chi'(T)$  (observed < 4 K) measured at 0 T  $H_{dc}$  remains nearly unaffected by the temperature sweep rates (figure 4(a)). Contrary to this, at 0.6 T  $H_{dc}$  AC  $\chi(T)$  measurement, the magnitude of  $\Delta\chi'_A(T)$  exhibits a linear relationship with temperature sweep rates (figure 4(b)). To better understand this behavior, figure 5 displays the temperature sweep rate dependence of  $\Delta\chi'_A(T)$  and its linear fit. Remarkably, the slope of the line changes with varying temperatures. Specifically, as the temperature decreases, the slope linearly increases up to  $\sim 2.5$  K, beyond which it decreases (see inset of figure 5). It has been found that slope of the line changes with varying the temperature. A similar trend was observed for temperature-dependent  $\Delta\chi'_A(T)$  in previous work [17]. These findings suggest that the magnitude of  $\Delta\chi'_A(T)$  is suppressed as the temperature increases.

Next, we performed the magnetic field-dependent AC susceptibility measurement ( $\chi(H)$ ) for DTO and HTO by sweeping the  $H_{dc}$  up to 1.5 T (and cycled back) at a constant temperature 4 K. Figure 6 shows the magnetic field-dependent real part of AC susceptibility ( $\chi'(H)$ ) measured at 98.3 Hz frequency and 1.5 Oe  $H_{ac}$  at 4 K. The measurements were carried out for DTO in three different magnetic sweep rate modes: stabilized, 50 Oe  $s^{-1}$ , and 100 Oe  $s^{-1}$ . In both the 50 Oe  $s^{-1}$  and 100 Oe  $s^{-1}$  continuous magnetic field sweep

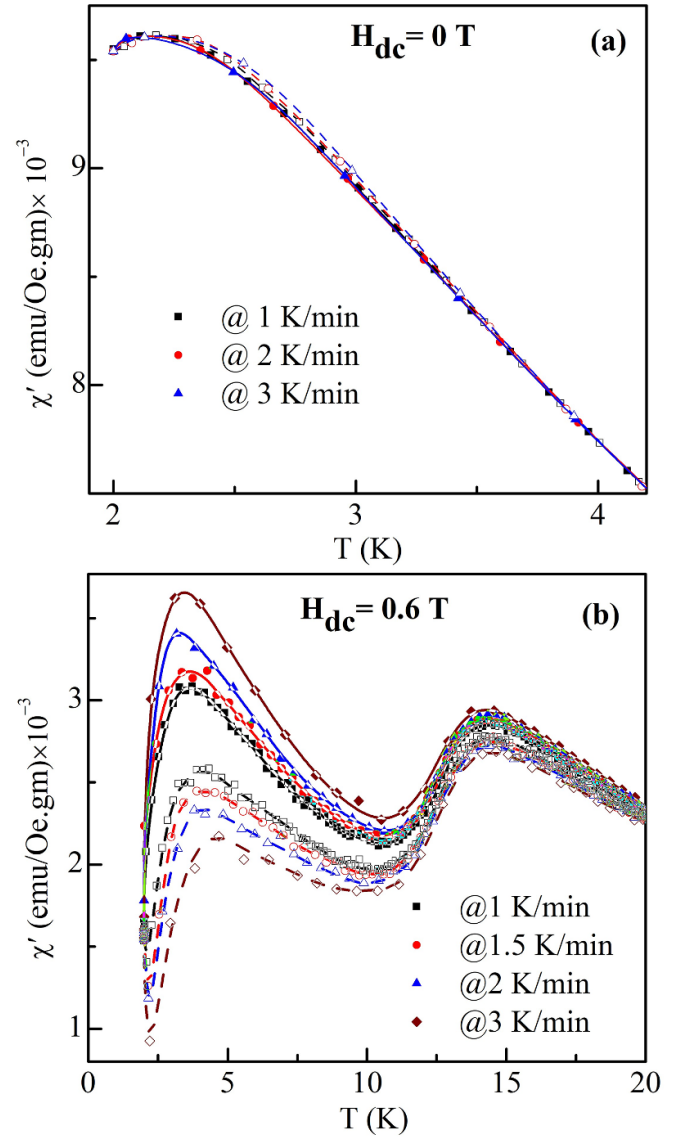


**Figure 4.** For  $Dy_2Ti_2O_7$ ; Temperature-dependent real part of AC susceptibility ( $\chi'(T)$ ) measured in FCC (solid symbol (with line as a guide to the eye)) and FCW (open symbol (with dashed line as a guide to the eye)) modes at 98.3 Hz and 1.5 Oe AC amplitude for different temperature sweep rates in the presence of 0 T (a) and 0.6 T (b) DC bias magnetic field.

mode, the measurements show magnetic hysteresis between the forward and backward modes. Whereas in the stabilized mode measurement, where measurement occurs after stabilization of the magnetic field at each set point, we do not observe any magnetic hysteresis. The value of magnetic hysteresis ( $\Delta\chi'(H)$ ) is calculated as the difference between the forward and backward  $\chi'(H)$ , i.e.,  $\Delta\chi'(H) = \chi'(H)_{Forward} - \chi'(H)_{Backward}$ . Notably, we made interesting observations during the backward (1.5 T  $\rightarrow$  0 T) magnetic field sweeping at both 50 Oe  $s^{-1}$  and 100 Oe  $s^{-1}$  sweep rates. A crossover point was observed at  $\sim 0.1$  T, below which  $\Delta\chi'(H)$  changed its sign, akin to the behavior of  $\Delta\chi'(T)$ .

Figure 6(b) shows the magnetic field sweep rate dependent variation in  $\Delta\chi'(H)$  at 4 K for different magnetic fields



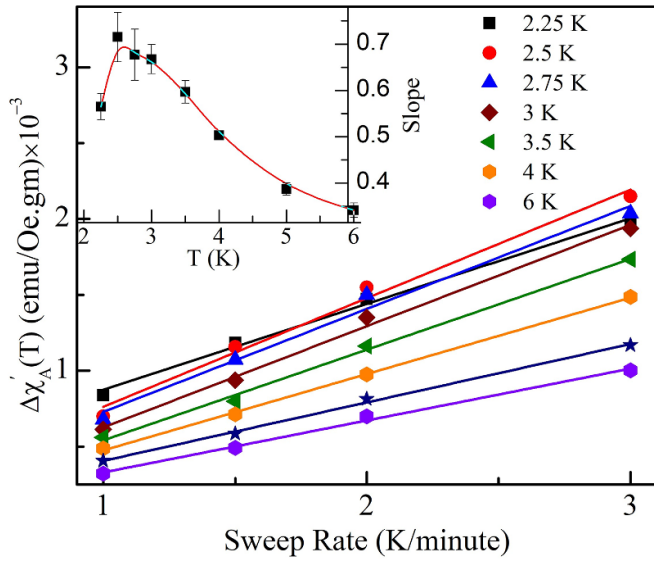


**Figure 5.** For  $\text{Dy}_2\text{Ti}_2\text{O}_7$ ; Temperature sweep rate dependent variation in anomalous thermal hysteresis ( $\Delta\chi'_A(T)$ ) measured at 0.6 T DC bias magnetic field and its linear fit at different temperatures. Inset shows the temperature-dependent variation in the slope obtained from the linear fit.

for DTO. Interestingly, up to 0.15 T,  $\Delta\chi'(H)$  exhibits a complex behavior, characterized by a decrease in the magnitude at higher magnetic field sweep rates. At higher magnetic fields ( $>0.15$  T),  $\Delta\chi'(H)$  shows a linear increase with magnetic field sweep rate akin to the  $\Delta\chi'_A(T)$  variation with temperature sweep rate. A similar behavior is observed for HTO and provided in figure S7(a) of the supplemental information file. For further investigation, we conduct  $\chi(H)$  in forward and backward modes at 1.5 Oe  $H_{ac}$  for 98.3 Hz and 498.3 Hz frequencies. Inset of figure 6(a) illustrates the  $\chi'(H)$  variation in forward and backward sweep modes at 98.3 Hz and 498.3 Hz frequencies. Notably, frequency shows significant impact on the magnitude of  $\Delta\chi'(H)$ , akin to the behavior of  $\Delta\chi'_A(T)$  with varying AC variable. These findings confirm that, just like the dependency of  $\Delta\chi'_A(T)$  on AC variables and temperature sweep rate,  $\Delta\chi'(H)$  also exhibits a dependency on the AC variables ( $f$ ) and magnetic field sweep rate.

To investigate the influence of temperature on  $\Delta\chi'(H)$ , we performed the cyclic  $\chi(H)$  measurements at different temperatures. Figure 7(a) shows the magnetic field-dependent  $\chi'(H)$  measured in forward and backward sweep modes at different temperatures. The measurement depicts that crossover in the  $\Delta\chi'(H)$  occurs only  $\geq 4$  K. For clarity, we have shown it in the inset of figure 7(a). A similar observation has been observed in HTO and given in figure S6 of the supplemental information file. Furthermore, in figure 7(b), we have shown the temperature-dependent variation in  $\Delta\chi'(H)$  at different magnetic fields for DTO. At 0.05 T magnetic field,  $\Delta\chi'(H)$  exhibits positive values below 4 K, but above this threshold, it undergoes a sign change up to 0.15 T magnetic field. For higher magnetic field,  $\Delta\chi'(H)$  do not show any crossover and exhibits a linear behavior with temperature.

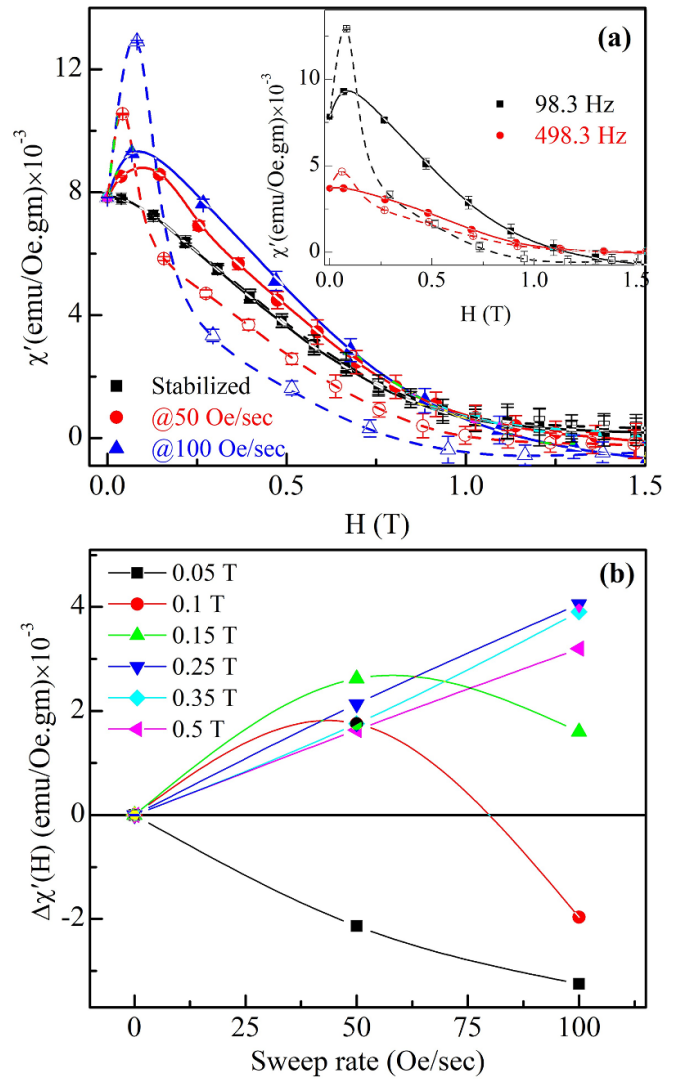


**Figure 6.** For  $\text{Dy}_2\text{Ti}_2\text{O}_7$ ; (a) Magnetic field-dependent real part of AC susceptibility ( $\chi'(T)$ ) measured in forward  $0 \rightarrow 1.5$  T (solid symbol (with line as a guide to the eye)) and backward  $1.5 \rightarrow 0$  T (open symbol (with dashed line as a guide to the eye)) modes at 98.3 Hz and 1.5 Oe in stabilized, 50 Oe  $s^{-1}$ , and 100 Oe  $s^{-1}$  sweep rates at 4 K. Inset shows the  $\chi'(H_{dc})$  measured in forward and backward field sweep modes for 98.3 Hz and 498.3 Hz frequencies at 4 K. (b) Magnetic field sweep rate-dependent variation in the magnetic hysteresis ( $\Delta\chi'(H)$ ) measured at different magnetic fields at 4 K.

The observed temperature and magnetic field sweep rate dependence of anomalous hysteresis indicates that the existing phonon-mediated spin-flipping mechanism [25–28] gets altered by biased  $H_{dc}$ . For investigation, we performed the temperature- and magnetic field-dependent dielectric permittivity ( $\epsilon$ ) measurement for DTO. Figure 8(a) shows the temperature-dependent real part of dielectric permittivity ( $\epsilon'(T)$ ) measured at different  $H_{dc}$ . In the  $\epsilon'(T)$  plot (figure 8(a)), we observe two successive relaxations at  $\sim 7.5$  K and 4 K. Furthermore, below 4 K, we observed thermal hysteresis between cooling and warming measurement mode, similar to the  $M(T)$  and  $\chi'(T, H_{dc} = 0$  T) magnetic measurements. The

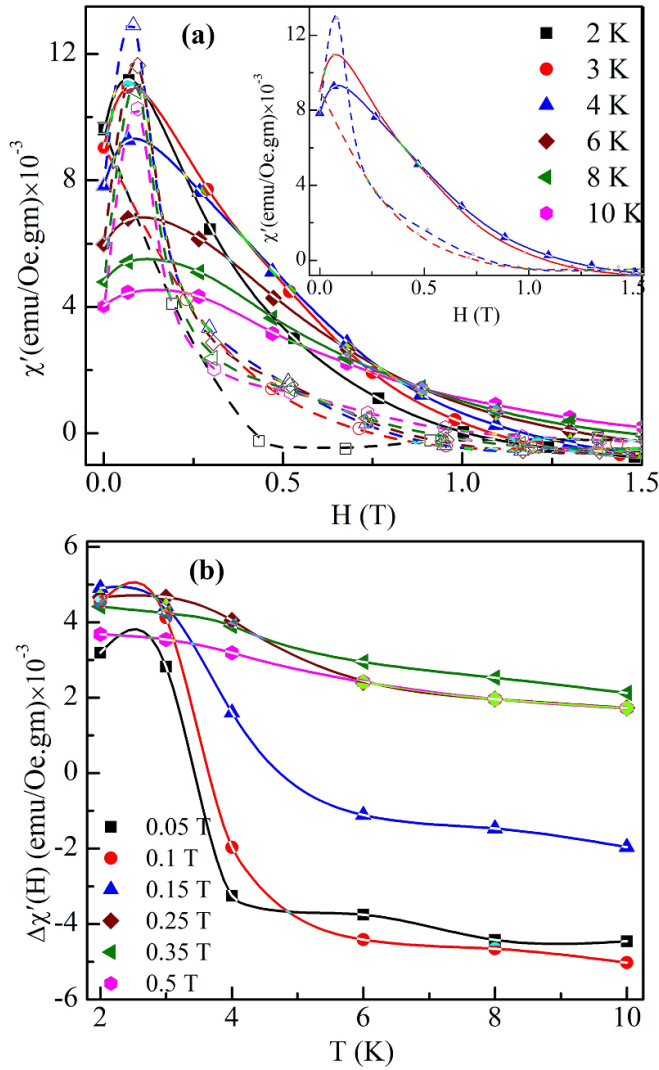


**Figure 7.** For  $\text{Dy}_2\text{Ti}_2\text{O}_7$ ; (a) Magnetic field-dependent real part of AC susceptibility ( $\chi'$ ) measured in forward  $0 \rightarrow 1.5$  T (solid symbol (with line as a guide to the eye)) and backward  $1.5 \rightarrow 0$  T (open symbol (with dashed line as a guide to the eye)) magnetic field sweep modes at 98.3 Hz frequency and 1.5 Oe AC amplitude for different temperatures. Inset shows the emergence of crossover at  $\sim 0.2$  T in forward and backward  $\chi'(H)$  measured at 4 K. (b) Temperature-dependent variation in  $\Delta\chi'$  at different DC magnetic fields.

application of  $H_{dc}$  causes an abrupt increase in the magnitude of  $\epsilon'(T)$ , along with a slight shift in both relaxation temperatures towards the higher temperature. As  $H_{dc}$  increases further, the thermal hysteresis in  $\epsilon'(T)$  expands its temperature range, while its magnitude gradually decreases. Figure 8(b) shows the magnetic field-dependent real part of dielectric permittivity ( $\epsilon'(H)$ ) measured at different temperatures. In this measurement,  $\epsilon'(H)$  exhibits a spontaneous increase with the magnetic field, reaching saturation above a critical field that depends on temperature. This abrupt increment in  $\epsilon'$  starts at 0.05 T magnetic field and saturates  $\leq 0.5$  T for measured temperature. Along with this, forward and backward magnetic field sweep mode shows hysteresis in the  $\epsilon'(H)$ . However, this hysteresis diminishes with increasing temperature and disappears

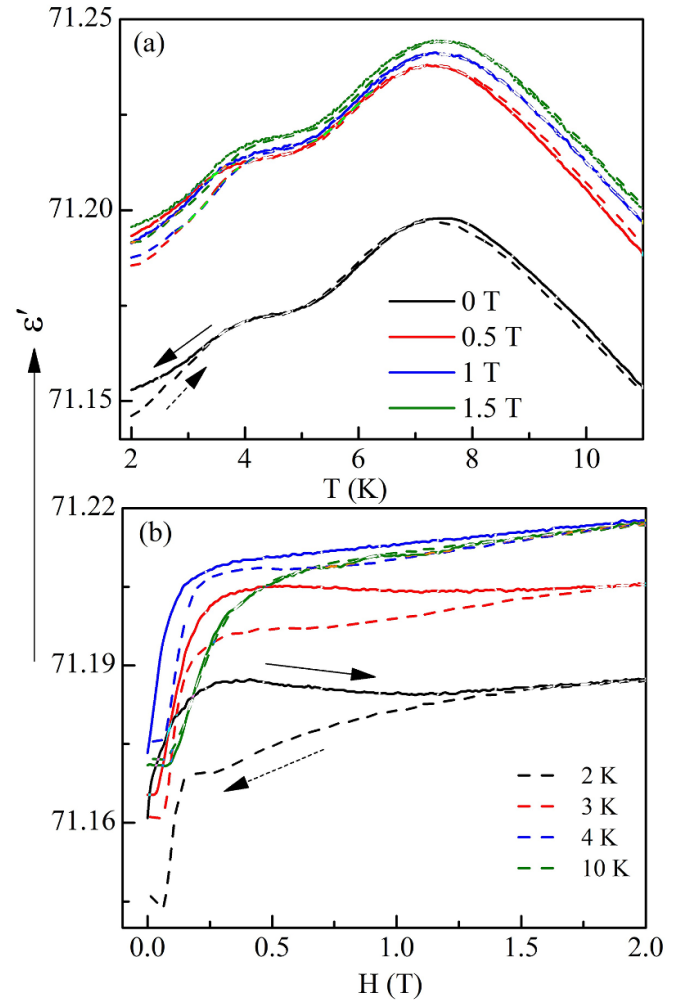


**Figure 8.** (a) Temperature-dependent real part of dielectric permittivity ( $\epsilon'$ ) measured in cooling (solid line) and warming (dashed line) modes @  $2 \text{ K min}^{-1}$  sweep rate at different DC magnetic fields and (b) magnetic field-dependent  $\epsilon'$  measured in forward ( $0 \rightarrow 2$  T, solid line) and reverse ( $2 \rightarrow 0$  T, dashed line) modes at different temperatures @  $100 \text{ Oe s}^{-1}$  sweep rate, for  $\text{Dy}_2\text{Ti}_2\text{O}_7$  at 50 kHz frequency.

at 10 K. The emergence of thermal and magnetic hysteresis in  $\epsilon'$  below 4 K confirms a strong interconnection of  $\epsilon'$  with local spin structure and spin dynamics, which are influenced by  $H_{dc}$ . The spontaneous increase in the  $\epsilon'$  with magnetic field suggest the suppression in the phonon-mediated-spin flipping mechanism. These findings indicate the alterations in the dielectric permittivity behavior due to the applied magnetic field, shedding light on the intricate interplay of  $\epsilon'$  with the spin-related phenomena.

#### 4. Discussion

The experimental results presented above clearly demonstrate the dependence of hysteresis on the measurement protocol in both DTO and HTO. The thermal hysteresis observed in  $M(T)$  (figure S2) and  $\chi'(T, H_{dc} = 0 \text{ T})$  (figures 1, 4 and S3) remains unaffected by the temperature sweep rate and AC

variables below 4 K. On application of  $H_{dc}$ , thermal hysteresis observed in  $M(T)$  gets suppressed, whereas in  $\chi'(T)$ , it causing an abrupt expansion in  $\Delta\chi'_A(T)$  within the measured temperature range (figure 2). The emergence of anomalous hysteresis with magnetic field, along with the linear decrease in the magnitude of  $\Delta\chi'_A(T)$  with temperature, suggest that increasing thermal energy diminishes the phenomena responsible for observed behavior. The thermal dependency of the anomalous hysteresis indicates its connection with underlying spin–phonon coupling, likely suppressed by  $H_{dc}$ . This suppression is consistent with the findings of Turrini *et al* [29] and Ozerov *et al* [30], who observed a suppression in spin-phonon coupling by the magnetic field. The spontaneous increase in  $\epsilon'$  with  $H_{dc}$  (figure 8) suggests a weakening in the magnetoelastic coefficient caused by the suppression in the phonon-mediated-spin flipping by applied  $H_{dc}$ . Scharffe *et al* [31] findings shows a decrease in the thermal conductivity coefficient with magnetic field in both DTO and HTO, further supporting this argument.

The impact of  $H_{dc}$  on existing spin–phonon coupling is evident from these findings, but its role in the emergent dynamic memory effect observed in AC susceptibility remains unanswered. Previous low-temperature studies on single crystals have demonstrated the breaking of the spin ice state into kagome ice ( $<1$  T) and 3in-1out or 1in-3out ( $>1$  T) on the application of the magnetic field along the [111] axis. Whereas, system retains its spin ice state for the field acting along [100] and [110] axes. It happens due to the existing crystal field anisotropy acting along  $<111>$  direction. When a magnetic field is applied along the [111] axis, the Zeeman splitting energy ( $\Delta E$ ) of the Ising doublet state undergoes a notable change for a quarter of the Ising spins that align parallel to the applied [111] axis within the corner shared tetrahedra. In contrast, the magnetic field acting along the [100] or [110] axis affects  $\Delta E$  of all Ising spins without affecting the spin ice ground state [21, 32, 33]. In the present study, due to the polycrystalline nature of the sample, DC bias magnetic field acts on the non-collinear Ising spin matrix along all possible directions, resulting in a complex ground state exhibiting both kagome ice and spin ice states at 0.6 T  $H_{dc}$ . In this complex state,  $\Delta E$  of the Ising doublet states have a relatively wide range of energy distribution compared to the single crystal. As a consequence, applied  $H_{dc}$  leads to the formation of random quenched disorder sites in the Ising spin matrix, which have larger spin relaxation times and a wide distribution [34]. These quenched disorder sites hinder the dynamical pathway of the ideal system and provide a limited path for spin-flipping. Due to this restriction, the system takes more time to achieve thermal equilibrium from an out-of-equilibrium state. The suppression in the spin-phonon coupling also suggests that quenched spins sites do not participate in the phonon-mediated spin flipping mechanism, supporting the increased out-of-equilibrium time duration caused by applied  $H_{dc}$ .

Remarkably, in all  $H_{dc}$  biased  $\chi'(T)$  measurements, we do not observe any significant change in the freezing temperatures in both FCC and FCW modes. It indicates that the resonant frequency of the cooperative spins at freezing points remains same in both measurement modes. Further, the exponential

increase in the magnitude of  $\Delta\chi'_A(T)$  with decreasing frequency, indicating the existence of another time region (with a large spin relaxation time) in the out-of-equilibrium state. A recent study has brought to light that below 1 K, thermally excited magnetic monopoles in the spin ice ground state blocks the dynamics of the quarter of spins. These spins exhibit a slower spin relaxation time compared to other spins and responsible for the low-temperature divergence in the spin relaxation time. Consequently, the system falls into the out-of-equilibrium state and magnetic monopoles exhibits fractal growth on a short time scale [14]. These findings support the presence of two or more relaxation regimes in these systems. In our present study, the temperature and magnetic field sweep rates dependent measurements also demonstrate the decay of  $\Delta\chi'(T, H_{dc})$  in a short time  $t$ . It indicates that in the out-of-equilibrium state, field-induced quench disorder sites develop a dynamic spin-correlation of larger  $\tau$  and exists for a shorter time  $t$  [15]. This field-induced dynamic correlation additionally contributes to the  $\chi'$  in out-of-equilibrium state and  $\chi'(T, H_{dc})$  can be represented as a sum of stationary part ( $\chi'_{ST}$ ) and non-stationary part ( $\chi'_{NST}$ ) [35]:

$$\chi'(\omega, t) = \chi'_{ST} + \chi'_{NST}. \quad (3)$$

The  $\chi'_{NST}$  contribution in  $\chi'$  is decided by the value of  $\tau$  with respect to some characteristic time ( $\tau_{char}$ ) at constant temperature and  $H_{dc}$ . When  $\tau \geq \tau_{char}$ , dynamics is non-stationary leading to a non-zero  $\chi'_{NST}$ , whereas for  $\tau \leq \tau_{char}$ , dynamics remains stationary, resulting a zero  $\chi'_{NST}$ . In temperature and magnetic field-dependent AC  $\chi$  measurement, we observe that the value of  $\chi'_{NST}$  is  $\frac{\Delta\chi'_A}{2}$ . The magnitude of  $\chi'_{NST}$  becomes non-zero and positive when  $k_B T$  decreases (FCC in  $\chi'(T)$ ) or  $\Delta E$  increases (increasing  $H_{dc}$  in  $\chi'(H)$ ). Conversely, the magnitude of  $\chi'_{NST}$  becomes non-zero and negative when  $k_B T$  increases (FCW in  $\chi'(T)$ ) or  $\Delta E$  decreases (decreasing  $H_{dc}$  in  $\chi'(H)$ ). The observed sign change in  $\chi'_{NST}$ , dependency of  $\Delta\chi'_A(T, H_{dc})$  on  $k_B T$  and AC variables indicate that the single-ion quantum tunneling process of Ising spins are coherently correlated in the out-of-equilibrium state [15, 36–38]. As a result, the system attain a memory of the initial conditions [39–41]. However, previous studies have clearly shown the classical nature of spin relaxation in these systems, indicating the non-coherent nature of spin correlation [42]. Nonetheless, an in-depth experimental and theoretical investigation is necessary to explain the observed anomalous behavior.

In DTO, the emergence of crossover in  $\Delta\chi'(T, H_{dc} = 0$  T) below 2.5 K indicates that effective dipolar interaction behaves similarly to the biased  $H_{dc}$ . At this temperature,  $\Delta\chi'_A(T)$  most probably emerges from the quenched sites developed by thermally induced magnetic monopoles [14]. However, unlike the effect of  $H_{dc}$ , the decay time of the out-of-equilibrium state induced by magnetic dipolar interaction is considerably fast, and this phenomena is more clearly observable at millikelvin (mK) scale. This observation becomes more evident when examining the magnetic field-dependent AC  $\chi$  measurement (figures 7(a) and S7) of DTO and HTO. In these measurements, no crossover is observed below 4 K, leading to the conclusion that effective dipolar interaction also



contributes to the development of short decay time out-of-equilibrium dynamic spin-correlations. Consequently, when  $H_{dc}$  is absent, the out-of-equilibrium properties are observed at the mK scale, consistent with previous studies [9, 13, 43]. The absence of crossover in HTO for measured frequency and  $H_{ac}$  indicates a speedy decay time of the non-stationary part in the absence of  $H_{dc}$ , likely due to its faster spin dynamics, even at the mK scale. Under equilibrium conditions, these systems become state-independent and exhibits hysteresis in Ising paramagnetic to spin ice crossover regime. This hysteresis is nearly independent of thermal and non-thermal variables. Sakakibara *et al* [44], in their low-temperature magnetization study, observed two successive field-induced hysteresis below 0.36 K in DTO and concluded that the ice-rule-breaking spin-flip turns out to be a novel first-order transition resembling a liquid-gas type. Consequently, the thermal hysteresis observed in the equilibrium state might be of the liquid-gas type. However, unlike single crystal, where complete spin ice to 3in-1out or kagome ice crossover occurs [44], the randomly oriented polycrystalline sample likely undergo only partial spin crossover by the applied magnetic field. As a result, these materials show hysteresis in the magnetization and AC susceptibility measurements under equilibrium conditions.

## 5. Conclusions

Present study demonstrates the distinct behavior of cooperative spins dynamics in both the equilibrium and out-of-equilibrium states of DTO and HTO. In the equilibrium state, static and dynamic magnetic properties of both DTO and HTO show weak dependence on external thermal and non-thermal variables. Interestingly, both compounds exhibit a liquid-gas type hysteresis during interaction/magnetic field-driven partial crossover in the local spin structure when measured in the equilibrium state. Contrary to this, in the out-of-equilibrium state, we observe a magnetic field-induced thermomagnetic hysteresis solely in AC  $\chi(T, H)$ , which strongly relies on driving thermal and non-thermal variables. Dielectric measurements show an abrupt increment in the dielectric permittivity with the applied magnetic field ( $<0.5$  T), indicating that the magnetic field extends the out-of-equilibrium time span of cooperative spins by weakening the spin-phonon coupling strength. It has been suggested that applied  $H_{dc}$  generates quenched disorder sites in the non-collinear Ising spin metrics and develops a dynamic spin correlation with slow relaxation. These dynamic spin-correlations also contribute to  $\chi(T, H)$  when the system falls into the out-of-equilibrium state. Based on measurement protocol, the non-stationary part can exhibit both positive and negative values and becomes zero in equilibrium or deteriorating conditions. The temperature/magnetic field sweep rate dependence, generally observed for classical systems, shows the short decay time of the out-of-equilibrium state. The observed memory effect in the out-of-equilibrium state, along with its sensitivity to external stimuli, set a stage for understanding the other topologically frustrated materials for their potential future applications.

## Data availability statement

The data that support the findings of this study are openly available at the following URL/DOI: <https://drive.google.com/drive/folders/1zwKiFPyuPL5-yCde2outnkCKqPg2Jqy?usp=sharing>.

## Acknowledgments

P Y acknowledges the CSIR-HRDG, India, for providing funds for this project, and the authors acknowledge CIF, IIT (BHU) for collecting data in the Magnetic Properties Measurement System (MPMS).

## Conflict of interest

The authors declare that they have no known competing financial interests or personal relationships that could have appeared to influence the work reported in this paper.

## ORCID iDs

Pramod K Yadav  <https://orcid.org/0000-0002-2266-3070>

Rajnikant Upadhyay  <https://orcid.org/0000-0002-0921-203X>

Chandan Upadhyay  <https://orcid.org/0000-0002-8392-7236>

## References

- [1] Schuller I K, Frano A, Dynes R C, Hoffmann A, Noheda B, Schuman C, Sebastian A and Shen J 2022 Neuromorphic computing: challenges from quantum materials to emergent connectivity *Appl. Phys. Lett.* **120** 140401
- [2] Grollier J, Querlioz D, Camsari K Y, Everschor-Sitte K, Fukami S and Stiles M D 2020 Neuromorphic spintronics *Nat. Electron.* **3** 360–70
- [3] Li S, Kang W, Zhang X, Nie T, Zhou Y, Wang K L and Zhao W 2021 Magnetic skyrmions for unconventional computing *Mater. Horiz.* **8** 854–68
- [4] Heyderman L J 2022 Spin ice devices from nanomagnets *Nat. Nanotechnol.* **17** 435–6
- [5] Bramwell S T and Gingras M J P 2001 Spin ice state in frustrated magnetic pyrochlore materials *Science* **294** 1495–501
- [6] Gardner J S, Gingras M J P and Greedan J E 2010 Magnetic pyrochlore oxides *Rev. Mod. Phys.* **82** 53–107
- [7] Zvyagin A A 2013 New physics in frustrated magnets: spin ices, monopoles, etc *Low Temp. Phys.* **39** 901–22
- [8] Dem Hertog B C and Gingras M J P 2000 Dipolar interactions and origin of spin ice in ising pyrochlore magnets *Phys. Rev. Lett.* **84** 3430–3
- [9] Matsuhiro K, Paulsen C, Lhotel E, Sekine C, Hiroi Z and Takagi S 2011 Spin dynamics at very low temperature in spin ice  $Dy_2Ti_2O_7$  *J. Phys. Soc. Japan* **80** 123711
- [10] Jaubert L D C and Holdsworth P C W 2011 Magnetic monopole dynamics in spin ice *J. Phys.: Condens. Matter* **23** 164222
- [11] Snyder J, Ueland B G, Slusky J S, Karunadasa H, Cava R J, Mizel A and Schiffer P 2003 Quantum-classical reentrant relaxation crossover in  $Dy_2Ti_2O_7$  spin ice *Phys. Rev. Lett.* **91** 107201

- [12] Ehlers G, Cornelius A L, Fennell T, Koza M, Bramwell S T and Gardner J S 2004 Evidence for two distinct spin relaxation mechanisms in “hot” spin ice  $\text{Ho}_2\text{Ti}_2\text{O}_7$  *J. Phys.: Condens. Matter* **16** S635
- [13] Samarakoon A M et al 2022 Anomalous magnetic noise in an imperfectly flat landscape in the topological magnet  $\text{Dy}_2\text{Ti}_2\text{O}_7$  *Proc. Natl Acad. Sci. USA* **119** 2117453119
- [14] Hallén J N, Grigera S A, Tennant D A, Castelnovo C and Moessner R 2022 Dynamical fractal and anomalous noise in a clean magnetic crystal *Science* **378** 1218–21
- [15] Tomasello B, Castelnovo C, Moessner R and Quintanilla J 2019 Correlated quantum tunneling of monopoles in spin ice *Phys. Rev. Lett.* **123** 67204
- [16] Savary L and Balents L 2017 Disorder-induced quantum spin liquid in spin ice pyrochlores *Phys. Rev. Lett.* **118** 087203
- [17] Yadav P K and Upadhyay C 2020 Signature of correlated quantum tunneling and thermal dephasing in quantum-classical coupled  $\text{Ho}_2\text{Ti}_2\text{O}_7$  and  $\text{Dy}_2\text{Ti}_2\text{O}_7$  spin ices *J. Magn. Magn. Mater.* **498** 166133
- [18] Yadav P K, Tolkiehn M and Upadhyay C 2019 Dielectric relaxations in  $\text{Ho}_2\text{Ti}_2\text{O}_7$  and  $\text{Dy}_2\text{Ti}_2\text{O}_7$  pyrochlores *J. Phys. Chem. Solids* **134** 201–8
- [19] Yadav P K, Singh P, Shukla M, Banik S and Upadhyay C 2020 Effect of B-site substitution on structural, magnetic and optical properties of  $\text{Ho}_2\text{Ti}_2\text{O}_7$  pyrochlore oxide *J. Phys. Chem. Solids* **138** 109267
- [20] Yadav P K, Harijan P K, Tripathi A and Upadhyay C 2019 Effect of A-site Fe substitution on the magnetic behavior of  $\text{Dy}_2\text{Ti}_2\text{O}_7$  spin ice *J. Magn. Magn. Mater.* **481** 221–6
- [21] Fukazawa H, Melko R G, Higashinaka R, Maeno Y and Gingras M J P 2002 Magnetic anisotropy of the spin-ice compound  $\text{Dy}_2\text{Ti}_2\text{O}_7$  *Phys. Rev. B* **65** 054410
- [22] Tomasello B, Castelnovo C, Moessner R and Quintanilla J 2015 Single-ion anisotropy and magnetic field response in spin ice materials  $\text{Ho}_2\text{Ti}_2\text{O}_7$  and  $\text{Dy}_2\text{Ti}_2\text{O}_7$  *Phys. Rev. B* **92** 155120
- [23] Clancy J P, Ruff J P C, Dunsiger S R, Zhao Y, Dabkowska H A, Gardner J S, Qiu Y, Copley J R D, Jenkins T and Gaulin B D 2009 Revisiting static and dynamic spin-ice correlations in  $\text{Ho}_2\text{Ti}_2\text{O}_7$  with neutron scattering *Phys. Rev. B* **79** 014408
- [24] Ehlers G, Gardner J S, Qiu Y, Fouquet P, Wiebe C R, Balicas L and Zhou H D 2008 Dynamic spin correlations in stuffed spin ice  $\text{Ho}_{2+x}\text{Ti}_{2-x}\text{O}_{7-\delta}$  *Phys. Rev. B* **77** 052404
- [25] Saito M, Higashinaka R and Maeno Y 2005 Magnetodielectric response of the spin-ice  $\text{Dy}_2\text{Ti}_2\text{O}_7$  *Phys. Rev. B* **72** 144422
- [26] Ruminy M, Chi S, Calder S and Fennell T 2017 Phonon-mediated spin-flipping mechanism in the spin ices  $\text{Dy}_2\text{Ti}_2\text{O}_7$  and  $\text{Ho}_2\text{Ti}_2\text{O}_7$  *Phys. Rev. B* **95** 060414(R)
- [27] Katsufuji T and Takagi H 2004 Magnetocapacitance and spin fluctuations in the geometrically frustrated magnets  $\text{R}_2\text{Ti}_2\text{O}_7$  (R=rareearth) *Phys. Rev. B* **69** 064422
- [28] Yadav P K and Upadhyay C 2019 Magnetodielectric relaxation in  $\text{Ho}_2\text{Ti}_2\text{O}_7$  and  $\text{Dy}_2\text{Ti}_2\text{O}_7$  Spin Ice *J. Supercond. Nov. Magn.* **32** 2267–73
- [29] Turrini A A, Ruminy M, Bourdarot F, Stuhr U, White J S, Tucker G, Skoulatos M, Núñez-Valdez M and Fennell T 2021 Magnetic-field control of magnetoelastic coupling in the rare-earth pyrochlore  $\text{Tb}_2\text{Ti}_2\text{O}_7$  *Phys. Rev. B* **104** 224403
- [30] Ozerov M, Anand N, van de Burgt L J, Lu Z, Holleman J, Zhou H, McGill S and Beekman C 2022 Magnetic field tuning of crystal field levels and vibronic states in the spin ice compound  $\text{Ho}_2\text{Ti}_2\text{O}_7$  observed with far infrared reflectometry *Phys. Rev. B* **105** 165102
- [31] Scharffe S, Kolland G, Valldor M, Cho V, Welter J F and Lorenz T 2015 Heat transport of the spin-ice materials  $\text{Ho}_2\text{Ti}_2\text{O}_7$  and  $\text{Dy}_2\text{Ti}_2\text{O}_7$  *J. Magn. Magn. Mater.* **383** 83–87
- [32] Tabata Y, Kadowaki H, Matsuhira K, Hiroi Z, Aso N, Ressouche E and Fåk B 2006 Kagomé ice state in the dipolar spin ice  $\text{Dy}_2\text{Ti}_2\text{O}_7$  *Phys. Rev. Lett.* **97** 257205
- [33] Mostame S, Castelnovo C, Moessner R and Sondhi S L 2014 Tunable nonequilibrium dynamics of field quenches in spin ice *Proc. Natl Acad. Sci. USA* **111** 640–5
- [34] Budrikis Z, Politi P and Stamps R L 2012 A network model for field and quenched disorder effects in artificial spin ice *New J. Phys.* **14** 045008
- [35] Busiello G 2013 Out-of-equilibrium dissipative ac-susceptibility in quantum ising spin glass *J. Mod. Phys.* **4** 784–90
- [36] Magazzù L, Forn-Díaz P, Belyansky R, Orgiazzi J L, Yurtalan M A, Otto M R, Lupascu A, Wilson C M and Grifoni M 2018 Probing the strongly driven spin-boson model in a superconducting quantum circuit *Nat. Commun.* **9** 1403
- [37] Gartner M, Bohnet J G, Safavi-Naini A, Wall M L, Bollinger J J and Rey A M 2017 Measuring out-of-time-order correlations and multiple quantum spectra in a trapped-ion quantum magnet *Nat. Phys.* **13** 781–6
- [38] Chille V, Quinn N, Peuntinger C, Croal C, Mišta L, Marquardt C, Leuchs G and Korolkova N 2015 Quantum nature of Gaussian discord: experimental evidence and role of system-environment correlations *Phys. Rev. A* **91** 050301(R)
- [39] Yadin B, Bogaert P, Susa C E and Girolami D 2019 Coherence and quantum correlations measure sensitivity to dephasing channels *Phys. Rev. A* **99** 012329
- [40] Editorial 2018 New horizons towards thermalization *Nat. Phys.* **14** 969
- [41] Hu M L, Hu X, Wang J, Peng Y, Zhang Y R and Fan H 2018 Quantum coherence and geometric quantum discord *Phys. Rep.* **762–764** 1–100
- [42] Bovo L, Bloxson J A, Prabhakaran D, Aeppli G and Bramwell S T 2013 Brownian motion and quantum dynamics of magnetic monopoles in spin ice *Nat. Commun.* **4** 1535
- [43] Paulsen C, Jackson M J, Lhotel E, Canals B, Prabhakaran D, Matsuhira K, Giblin S R and Bramwell S T 2014 Far-from-equilibrium monopole dynamics in spin ice *Nat. Phys.* **10** 135–9
- [44] Sakakibara T, Tayama T, Hiroi Z, Matsuhira K and Takagi S 2003 Observation of a liquid-gas-type transition in the pyrochlore spin ice compound  $\text{Dy}_2\text{Ti}_2\text{O}_7$  in a magnetic field *Phys. Rev. Lett.* **90** 207205